Passive SAR Satellite System (PASSAT)

Atkinson, George; Sayin, Alp; Stove, Andrew; Underwood, C.I.; Cherniakov, Mikhail; Antoniou, Michail

DOI:
10.1049/iet-rsn.2018.5225

Passive SAR Satellite System (PASSAT): airborne demonstrator and first results

George Atkinson[1], Alp Sayin[1], Andrew Stove[1], Craig I Underwood[2], Mikhail Cherniakov[1], Michael Antoniou[1*]
[1]Department of Electronic, Electrical and Systems Engineering, University of Birmingham, Birmingham, United Kingdom
[2]Surrey Space Centre, University of Surrey, Surrey, United Kingdom
[*]m.antoniou@bham.ac.uk

Abstract - This paper presents the development and execution of an airborne experimental campaign as part of the continuing investigation of a passive Synthetic Aperture Radar using digital television broadcasting stations as illuminators of opportunity, and micro-/nano-satellite receivers in Low Earth Orbit. For the flight experiments, a hardware demonstrator was developed that utilised two receiving antennas, allowing both cross-correlation and auto-correlation range compression schemes, and was mounted to an airborne platform to image stationary rural areas up to 50 km from the transmitter. This paper presents the first image results of these experiments as well as initial analysis of image formation aspects including, range compression scheme and effects on the image quality of the signal to noise on the reference channel.

1. Introduction

Space-borne Synthetic Aperture Radar (SAR) has proven itself as a highly capable remote sensing technique over the last decade, with a plethora of applications [1–3]. There is also an increasing demand for persistent, or near-persistent, earth monitoring from a space-borne platform. However, such a system would require a large number of SAR satellites to achieve this. While there are a number of space-borne SAR systems already deployed, these systems come at substantial financial costs, ranging up to the hundreds of millions of pounds, to develop the technology and deploy the satellites into orbit. They also provide a time between updates which is typically several days. Thus, for an active constellation of satellites designed for the purpose of persistent monitoring, the high system complexity and cost restricts the number of active instruments that can be developed in practice.

One potential solution for a practical low-cost SAR constellation for persistent monitoring could be a passive, rather than active, system such as the Passive SAR Satellite constellation (PASSAT) concept [4]. Rather than large and expensive satellites carrying active transmitter elements, a passive SAR satellite would utilise ground-based transmitters of opportunity to reduce size and cost. Due to the passive nature of the satellites, the receiver, storage, and data downlink components would require only a small volume and could be accommodated by a nano-/micro-satellite (CubeSat standards). The smaller size, as well as the smaller power requirements, of a receive-only system means that the PASSAT system concept would be orders of magnitude cheaper and less complex than a constellation of active SAR satellites in a similar low earth orbit. To further reduce cost and complexity, the data collected by the satellites would be stored on-board, then transmitted to the ground for post-processing into an image. A visualization of the concept can be seen in Fig. 1.

Fig. 1 *Passat concept-art visual*

For the PASSAT system, the transmitters of opportunity are ground-based Digital Video Broadcasting – Terrestrial (DVB-T) transmission stations. Of all the possible ground-based illuminators of opportunity for passive SAR imaging, DVB-T provides the best properties, including a relatively high transmission power (10-250 kW of effective radiated power), as well as a bandwidth (7.6 MHz) which gives a range resolution of approximately 20 m for the best-case geometry. The preliminary investigation of the major system characteristics, such as resolution, sensitivity, satellite bus and payload have already been considered in [4]. Additionally, DVB-T SAR has already been shown to be fundamentally possible [5–9].

Previous concepts that have explored a generic passive radar system, which combine a space-borne and ground-based segments, have explored the opposite configuration to PASSAT, for example, passive SAR using navigation satellite transmitters and ground-based receivers has been considered at great length [10–17]. Conversely PASSAT

proposes the use of one or more ground-based transmitters and multiple space-borne receivers.

While conventional orbital SAR systems operate in the L- to X-band, DVB-T operates in the VHF/UHF region, which is known for its foliage penetration and indirect propagation properties. Furthermore, the PASSAT concept as described is a bistatic system that can take advantage of bistatic scattering effects to increase available scene information [18], but can also result in unfavourable imaging geometries which result in a loss of spatial resolution. The analysis showed that this would only occur very rarely for all the transmitters which illuminate any scene and would thus not invalidate the PASSAT concept.

Recent work has shown the results of preliminary calculations of the range and cross-range resolutions, as well as the system sensitivity, for a theoretical PASSAT system in a number of favourable and unfavourable geometries [19]. Because the system is bistatic and dynamic, the resolution is dependent on the acquisition geometry, which changes as the satellite receivers move in orbit. An example passive low earth orbit constellation was simulated to determine the worst-case resolution and the frequency of occurrence of forward scatter events, where range resolution would be lost altogether. In parallel, a baseline system on-board a 12-U CubeSat was designed and options for a constellation of these satellites were evaluated [20].

The bistatic nature of this system, as well as the UHF frequencies used by DVB-T present an interesting combination of properties for forming and interpreting SAR images. Before we can consider a space-borne system, we first need to understand how to form DVB-T SAR images in such an environment, and to understand what we can gain from these images. To this end, an appropriate technology demonstrator was developed to form DVB-T SAR images in a bistatic environment [21]. This demonstrator was tested during a series of ground trials in a quasi-monostatic configuration with the transmitter. The trials utilised a straight road 20 km away from the transmitter and produced images at ranges up to 5km from the receiver.

The next logical step then, and the goal of the work described in this paper, is to use the demonstrator to conduct experiments with an airborne platform, to confirm its functionality, and begin a long-term experimental study to investigate generic DVB-T SAR aspects as well as elements specific to PASSAT. The paper is organised as follows: Section 2 describes the PASSAT demonstrator and the airborne campaign conducted. Section 3 presents images obtained and their validation. Finally, Section 4 shows a first investigation of image properties, including a comparison of different range compression techniques, and the effects of noise present in the reference signal used for range compression.

2. PASSAT demonstrator and airborne campaign

2.1. Receiving system and airborne platform

The demonstrator was based on a Universal Software Radio Peripheral (USRP) made by National Instruments, and programmed to receive DVB-T signals on two input channels (Fig.2). The two channels were connected to patch antennas, custom made to fit behind the windows of the aircraft, with measured beamwidths of approximately 50 degrees in each of the principal planes and a gain of around 8 dB. The antennas were connected to an RF front-end chain for amplification and band-pass filtering to reject out-of-band interference, built from off-the-shelf components.

The USRP down-converted incoming signals to baseband, storing digital I/Q samples to the internal, high-speed Solid State Drive (SSD) of a portable workstation. The position of the aircraft was recorded by an Advanced Navigation Spatial Fog, a high-precision GNSS aided Inertial Measurement Unit (IMU) which is capable of high update rates [22]. The Spatial Fog unit was connected to the same control computer and recorded the positional data to the same SSD. Synchronisation of the USRP with the Spatial Fog was done during post-processing, as both instruments have their own GPS-disciplined oscillators and provide measurement timestamps.

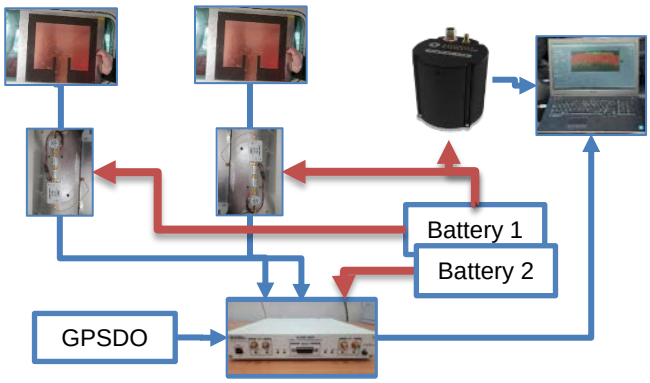

***Fig. 2** Hardware Block Diagram for Airborne Receiver*

The radar electronics were mounted within a shock-resistant case for airborne trials. A photograph of the receiver is shown in Fig. 3.

***Fig. 3** Flight- ready system*

The airborne platform was a 4-seat Cessna 172N Skyhawk aircraft. The two receiving antennas were placed on either side of the aircraft. One of them was used to record the direct signal from the transmitter (heterodyne channel), the other one pointing towards the target area (radar channel). Due to shortage of space, the GPS antenna of the IMU was positioned at the back of the plane, and the distance between that and the radar antennas was taken into account during image formation. The arrangement of the equipment within the aircraft can be seen in Fig. 4.

2.2. Target Areas and acquisition geometry

The DVB-T transmitter used was the Sutton Coldfield broadcasting station near Birmingham, UK, which is based on a 264 m tall mast on top of a hill. The target area was located nearly 46 km away from the transmitter. The location of the transmitter, the target area and the ground track of the aircraft is shown in Fig. 5. The total distance from the transmitter to the furthest target investigated was slightly over 51 km. Acquisitions in a quasi-monostatic configuration were made to make analysis of the obtained images easier. The target area was in the vicinity of the Bruntingthorpe Aerodrome and Proving Ground, near Leicester, UK, and off the M1 motorway. Apart from the airfield, the area is rural and contains farmlands surrounded by tree lines and hedge rows.

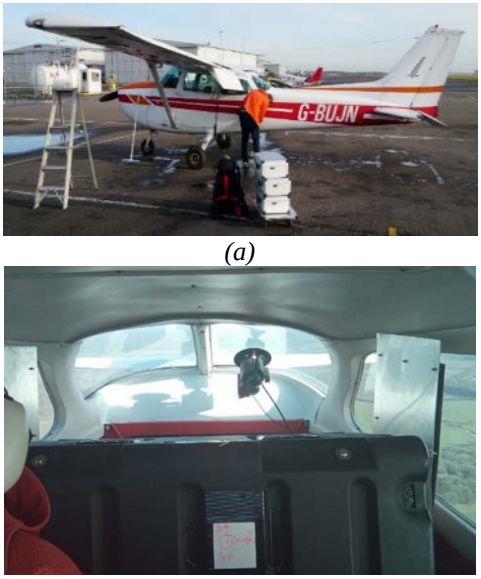

(a)

(b)

Fig. 4 *(a) airborne platform (b) equipment arrangement during flight*

The measurements were done at an aircraft altitude of 600 m above mean sea level, which is ~200 m above the top of Sutton Coldfield transmitter's aerials and ~500 m above ground level.

Fig. 5 *Satellite image of the Bruntingthorpe target area with the flight path of the aircraft shown (black line), and the distance and direction to the transmitter (white line), and the distance to the air field (yellow line)*

The measurements were done by recording a single DVB-T channel, centred at a frequency of 650 MHz. The experimental parameters are summarised in Table 1. Note that the bistatic angle is defined as the angle between the transmitter and receiver lines-of-sight and the centre of the target area.

2.3. Image formation

Bistatic SAR image formation typically involves the use of the direct signal from the transmitter to the receiver as a reference function for compressing radar echoes in range. However, for DVB-T, methods for providing this signal can vary. The optimal method is to decode the direct signal [23], and then locally re-construct it, resulting in a noise-free reference signal while supressing signal artefacts which may affect the DVB-T SAR imagery, such as DVB-T pilot signals, which in passive coherent location applications can otherwise introduce false detections.

Table 1 *Experiment Parameters*

Property	Value	Unit
Carrier Frequency	650	MHz
Bandwidth	7.6	MHz
Transmit Power	200	kW
Transmitter Mast Height	264	m
Transmitter Distance	45.1	km
Transmitter Grazing Angle	0.5	degrees
Rx Antenna Beamwidth	50	degrees
Bistatic Angle	4	degrees
Dwell Time	8	s
Average Ground Speed	240	km/h
Aircraft Heading	12	Degrees
Aircraft altitude (above mean sea level)	600	m

In airborne DVB-T SAR work so far, two different methods for providing range compression have been used. In the first one, the direct signal is recorded from a separate antenna pointed towards the transmitter, and is directly cross-correlated with radar data [5]. This provides a relatively clean version of the direct signal but requires an additional RF channel. The second method is based on the assumption that the direct signal is inadvertently collected by the radar antenna itself (most likely through its side-lobes, but that depends on the bistatic geometry). Therefore, range compression can be implemented simply by auto-correlating the radar data [6–8]. This method relies on the direct signal having a sufficient Signal-to-Noise Ratio (SNR), however it eliminates the need for an extra receiving channel. One limitation of this method is that artefacts will be produced in imagery since all radar echoes will in fact be correlated with all the others. If ratio between the direct signal and the strongest target is greater than that between the strongest target and the noise floor, then all these unwanted cross-correlations will be below the noise floor.

Crucially, the latter method is especially relevant to PASSAT, and might be the only option for providing range compression. First of all, decoding the direct signal from a fast-moving platform such as a satellite is not a first option due to the fact that multipath signals entering the reference channel will have a different Doppler shift from the direct signal which upsets an attempt to decode the signal [24]. Secondly, it has been calculated that for a sufficiently high SAR sensitivity, a receiving antenna of 15 dB gain can be

deployed from a nano-satellite [20]. At a satellite altitude of 400 km, the footprint of the antenna on the ground is so large that it is not possible to use separate antennas for direct and echo signal reception.

For the reasons above, range compression was tested during the trials for the cross-correlation and auto-correlation cases (Fig. 10), implemented in the frequency domain. This would allow us to assess any artefacts arising from auto-correlation, since to evaluate this at the theoretical level would be a formidable task due to the number of possible targets in a target area. After range compression, azimuth compression was performed with a standard back-projection algorithm [25], extended to the bistatic SAR case [26], taking the transmitter location and aircraft positional information from the IMU as inputs. In addition, the back-projection algorithm took into account the topography of the scene, using Digital Elevation Maps (DEMs) of the terrain, obtained via the Bing Maps free API.

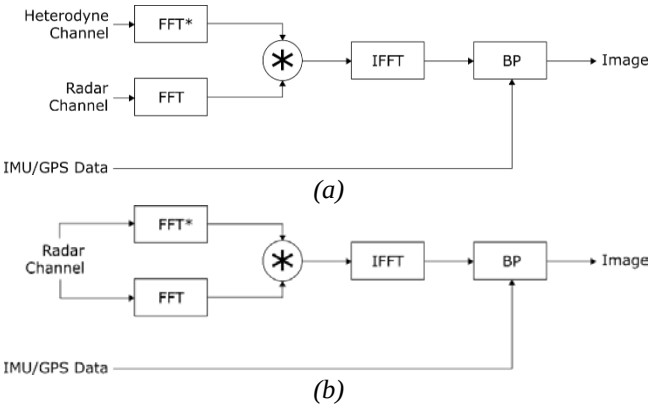

Fig. 6 *Correlation schemes for range compression (a) Cross-correlation scheme. (b) Auto-correlation scheme*

3. SAR images and verification

3.1. Comparison with ground truth

The SAR image from the target area is shown in Fig. 7. A satellite photograph of the area (taken from Bing Maps) is also shown above it for comparison. The image was formed with a dwell time of 8 s, corresponding to an overall aperture length of approximately 371 m, and with the cross-correlation method described above. This dwell time was chosen as it provided the longest aperture such that the resulting SAR image is focused without the need for motion compensation.

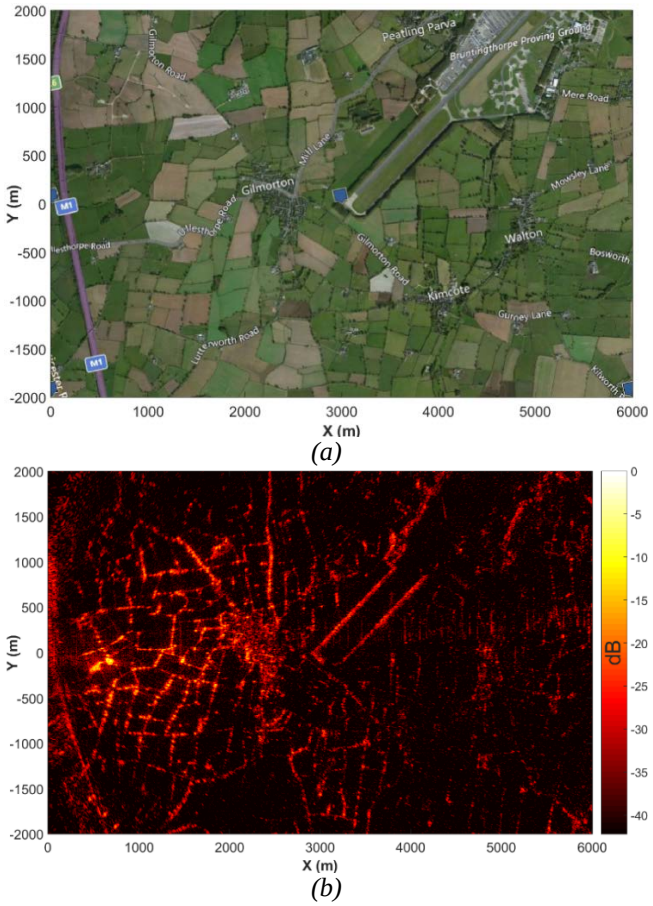

Fig. 7 (a) Satellite image (Bing Maps) of Bruntingthorpe measurement area, (b) SAR image with 8s dwell time

The colour scale is in dB, with 0 dB representing the maximum compressed echo intensity. The dynamic range of the image was clipped to 40 dB, which is just above the noise floor. The x-axis represents forward ground range from the receiver, while the y-axis is cross-range and is aligned to the flight direction of the aircraft.

It is significant to note that although the grazing angle to the receiver was about six degrees, i.e. about the minimum for which reasonable microwave SAR imagery can be obtained, without excessive shadowing, the grazing angle from the transmitter was of the order of 0.6 degrees and the quality of the imagery obtained shows that a lot of the scene would have been illuminated by indirect propagation, i. e. by diffraction, which is what would indeed be expected at these low frequencies from the way in which television signals propagate to television receivers.

A good accordance between the SAR image (Fig. 7 (b)) and the photograph (Fig. 7 (a)) can be observed. In particular, locations of high echo intensity coincide with the locations and orientations of trees, hedgerows and buildings in the image (e.g. Fig. 8, which is an enlargement of the target area up to 2km range and within a 2km cross-range span). Reflections from terrain are not visible, but at the low grazing angles of the transmitter and the receiver this is as expected. Another part of the image that can be investigated is from Bruntingthorpe airport itself (Fig. 8 (c) and (d)). Hedgerows follow the outline of the airstrip, which are also visible in the SAR image. Additionally, there are points of high echo intensity in the SAR image which coincide with

the locations of aircraft parking spots in the middle of the airfield.

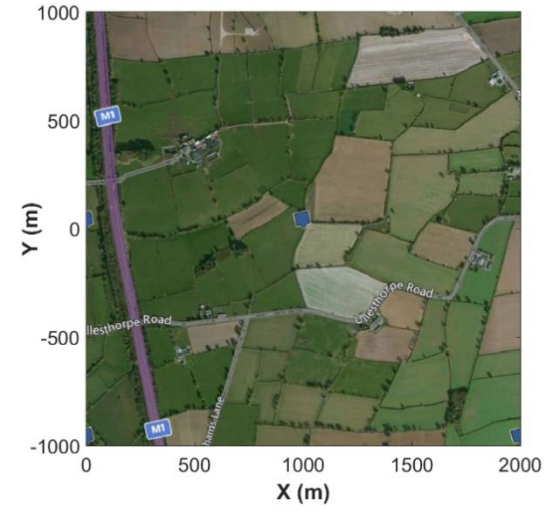

(a)

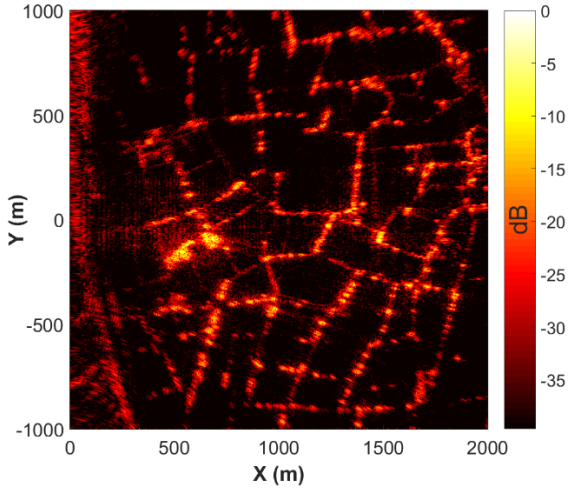

(b)

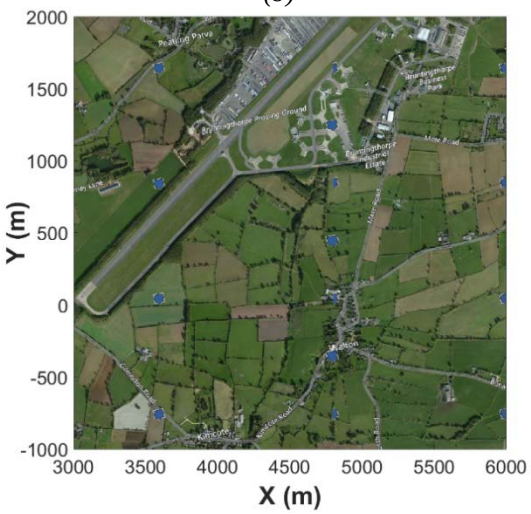

(c)

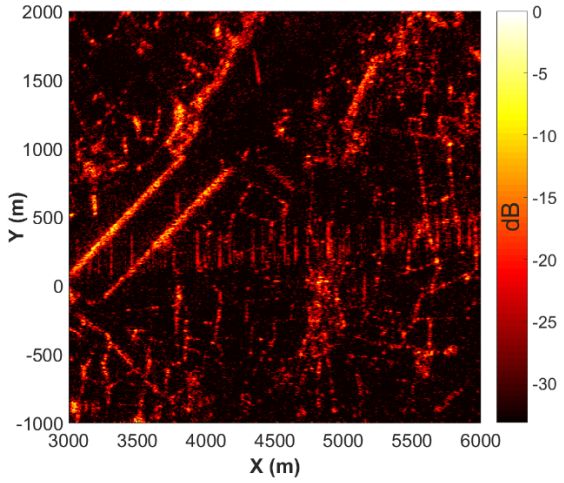

(d)

Fig. 8 *– Enlargement of target area. (a) Satellite image of first enlarged target area. (b) SAR image of target area shown in (a). (c) Satellite image of second enlarged target area. (d) SAR image of target area shown in (c)*

3.2. Point spread function analysis

To confirm the functionality of the image formation algorithm, point-like targets in the image should be analysed. For monostatic SAR, this can be done by placing calibrated targets such as corner reflectors in a scene. In our bistatic case, however, this becomes problematic due to bistatic scattering effects, and the need for a substantially large corner reflector due to the low 650 MHz carrier frequency. For these reasons, responses from in-scene targets whose response in our SAR image appears point-like (due to the spatial resolution) were sought. One such example was found in a wind turbine, whose response was extracted from the image and is shown in Fig. 9 (a). To compare its response to that of an ideal point target, a MATLAB simulation environment was created, where the DVB-T signal returns from a point target at the same location as the wind turbine could be generated under the same experimental setup described in Section 2. The simulated data were then processed with the same algorithm used to process the experimental data. The Point Spread Function (PSF) obtained in this case is shown in Fig. 9 (b). Comparing the simulated and experimental results, a significant resemblance between the two can be seen. To further illustrate this, cross-sections of the experimental and simulated responses were taken in the range and cross-range dimensions. The range cross-section results are shown in Fig. 9 (c), and the cross-range cross-sections are shown in Fig. 9 (d). In both results a very good coincidence between theory and experiment can be found, which validates the image formation algorithm used.

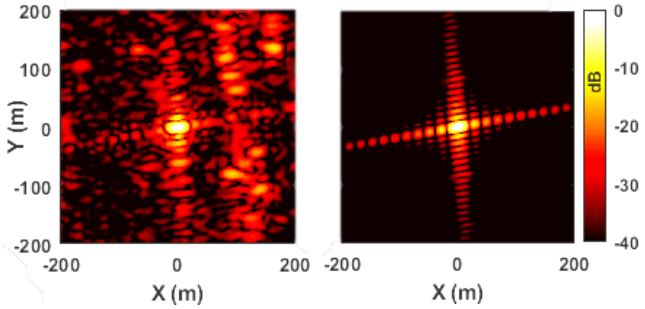

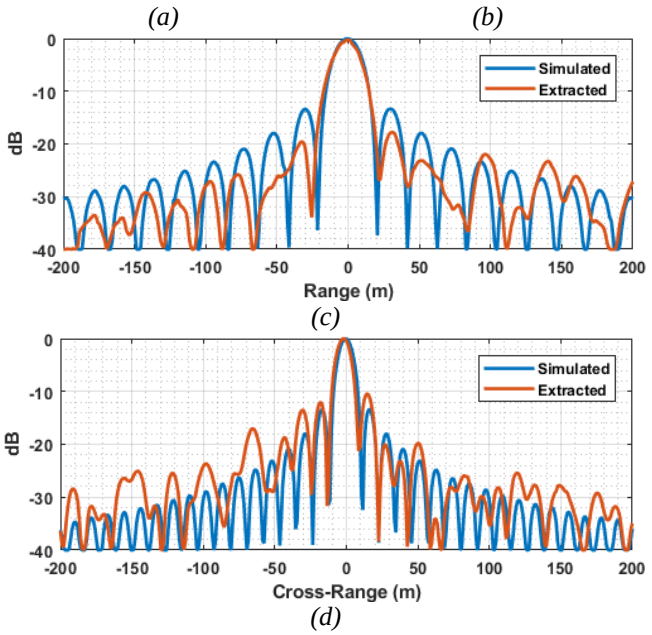

Fig. 9 *Experimental and simulated PSFs (a) Extracted PSF from experimental image. (b) Simulated PSF with same coordinates and as the extracted PSF in (a). (c) Comparison of range profiles. (d) Comparison of cross-range profiles*

4. Investigation of image characteristics

4.1. Comparison between range compression techniques

In Fig. 10, SAR images produced with auto-correlation and cross-correlation schemes in the first trial site with a dwell time of 8 s can be seen. There seems to be almost no difference in the image details between the images, so both seem acceptable, but with one notable exception; This is a straight line across the image obtained via auto-correlation, which corresponds to the side-lobes of the compressed direct path signal and can be seen between 0 and +500 m cross-range. This kind of effect is not new, as passive SAR images with GNSS also exhibit this property (see [10] or [11], for example), and some evidence of this may also be seen in other works, such as [6–8]. What merits further investigation is why this artefact is not seen in images obtained by cross-correlation, and how it can be removed without affecting information on real targets in the scene, which is part of future work. In addition, performing range compression via auto-correlation slightly increases the background level of the image. Specifically, the mean background level of the normalised SAR image is -42.1 dB in the auto-correlated result, and -45.4 dB in cross-correlated result, i.e. an increase of about 3 dB.

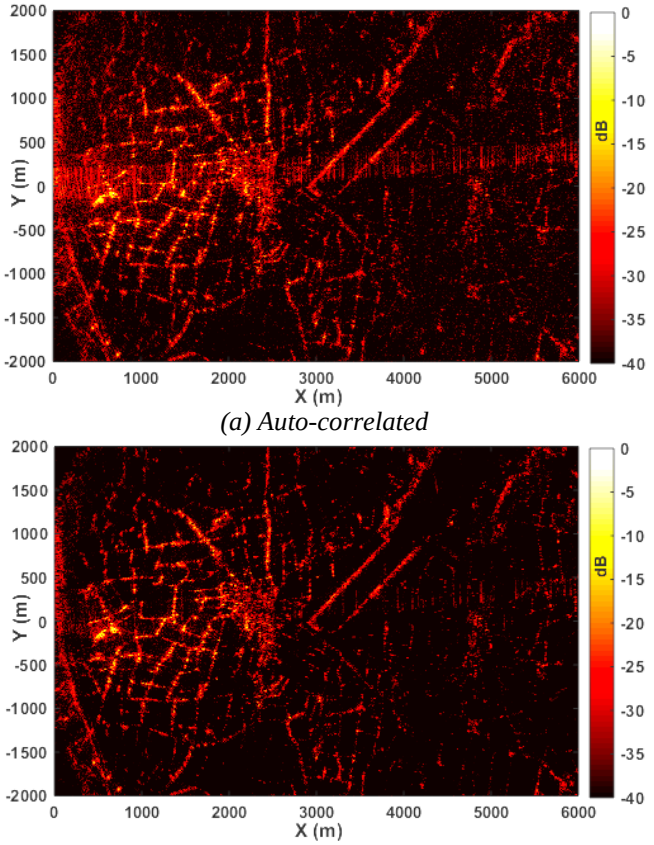

Fig. 10 *Comparison of autocorrelation and cross correlation schemes to obtain SAR images, images obtained via (a) auto-correlating the radar channel, (b) cross-correlating the radar channel with the reference channel*

4.2. Effects of Noise on the Reference Channel

An important aspect to consider is the effect of noise on the channel used for range compression purposes. This is because if the direct signal is not decoded, but is instead used as is for range compression, a degradation in image quality may be expected as the SNR on the direct signal decreases. This is relevant to airborne DVB-T SAR since this can be used to understand how far away the receiver can be from the transmitter and still acquire useful imagery (see for example [5], [6–8], where transmitter-receiver baselines can vary from a little over 10km up to several 10s of km). It is also relevant to the space-borne PASSAT concept because as the receiver is on a satellite, not only its distance to the receiver can be larger, but also the direct signal is likely to be radiated through the sidelobes of the transmitting antenna.

We can simulate this effect and the impact it has on SAR images using the measurement data from the flight trials. This can be done by adding white Gaussian noise to the direct signal recorded at the heterodyne channel, hence accordingly reducing its SNR to arbitrary levels. Then this direct signal can be cross-correlated with the radar signal for range-compression, and subsequently image formation, using the same method as the one shown in Fig. 6 (a). Figure 11 shows the effect of adding noise to a segment of the direct signal at the output of the receiving hardware. Its original SNR was measured to be 14 dB (Fig. 11 (a)). The SNR is calculated using the direct signal in frequency space, assuming that the space between successive DVB-T channels is pure noise. The SNR measured is then actually

(S+N)/N. But for a measurement of 14 dB, this is equivalent to an SNR of 13.8 dB, which is effectively the same within experimental error. As an example, in Fig. 11 (b), noise has been added to the direct signal of Fig. 11 (a) to emulate an SNR of -30 dB.

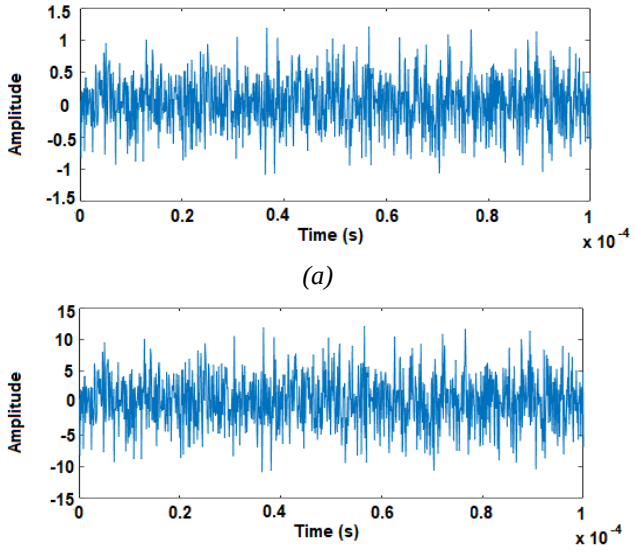

Fig. 11 *Segment of DVB-T direct signal (a) at the receiver output, (b) with added noise to emulate SNR of -30 dB*

Fig. 12 shows the results of image formation of a zoomed-in area from the Bruntingthorpe measurement after back-projection, with emulated direct signal SNRs as described above of -10, -20, and -30 dB. Fig. 12 (a) acts as the control and has no additional noise added. For each case, the colour scale of the plot is adjusted to the background power level of the image data. The background level is measured on the images, and therefore this includes any signal processing gain from the image formation algorithm itself.

Fig. 13 shows how the mean background level of the image in Fig. 12 (a) changes as the noise power added to the reference signal increases. The relationship is approximately linear between -5 and -30 dB SNR of the direct signal, and the trend is that an increase in noise power results in an increase in the mean background level, and therefore a decrease in overall image contrast. It is mentioned here that due to the very low grazing angles in this experiment, the background is noise limited rather than clutter (terrain) limited.

With a direct signal SNR of -10 dB the treelines and field boundaries identifiable in the original image are still visible, however some individual trees located within fields are obscured by noise. With an SNR of -20 dB, some of the field boundaries and treelines that could be identified are now lost to the noise, and individual trees are now indistinguishable to the background. By the time the direct signal SNR reaches -30 dB, only the brightest areas, usually clusters of trees or small forests, are distinguishable from the background noise level.

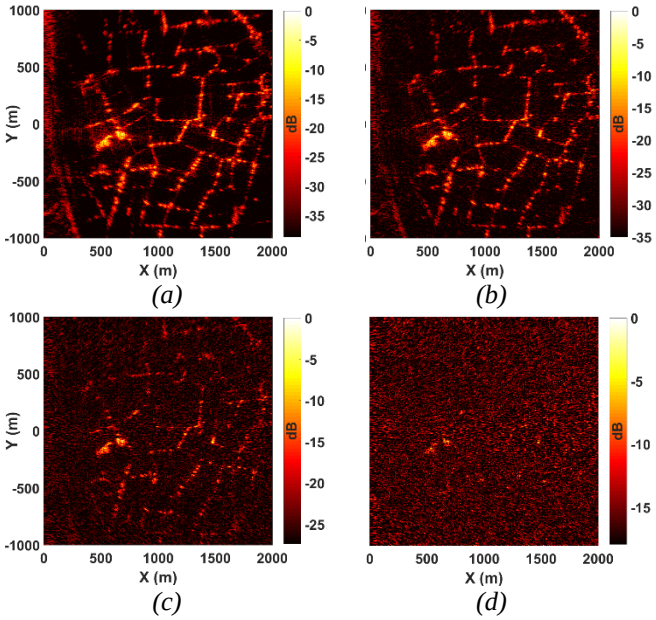

Fig. 12 *Extracts of back-projected SAR image with (a) direct signal SNR of 14 dB, (b) direct signal with added noise to emulate SNR of -10 dB, (c) direct signal with added noise to emulate SNR of -20 dB, (d) direct signal with added noise to emulate SNR of -30 dB*

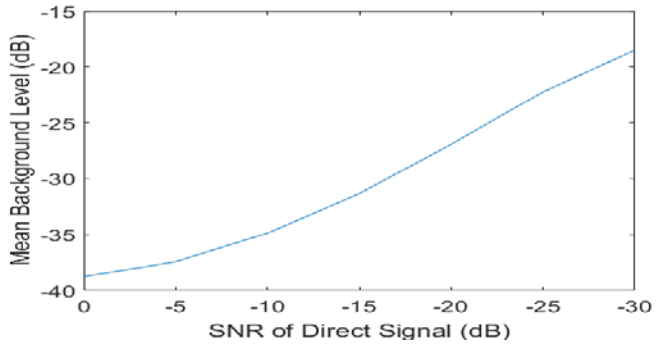

Fig. 13 *Graph showing the mean background level of the image in Fig. 12 (a) against the direct signal SNR with added noise before matched filtering.*

5. Conclusions

This paper summarised progress into the investigation of the PASSAT concept. An airborne technology demonstrator was built, and the first PASSAT airborne campaign was flown. Images were acquired, and the validity of the demonstrator and the image formation algorithms was confirmed. Aspects of SAR image formation in this configuration, such as means of performing range compression and the effects of SNR on the reference channel were considered. A small difference of 3 dB was observed between the background levels of images processed with an auto-correlation and cross-correlation range compression algorithm. This is likely due to the front-to-back ratio of the antennas used. Also of note is the observation of direct signal sidelobes within the image when processed with the auto-correlation scheme.

Further research is required to address aspects of the PASSAT technology for future development. For example, a fully realised PASSAT system would be bistatic, and therefore these geometries must be investigated. Previously in [19] a theoretical study of the PASSAT system sensitivity

showed that long-range operation is viable. The results of this paper show that images can be formed a distance of 50 km from the transmitter to the receiver, and also with additional noise reducing the SNR by 20 dB. Therefore, with a 6 dB doubling of range, combined with additional dwell time on target, these results provide confidence that images can be formed from a low earth orbit.

6. Acknowledgements

Work reported in this paper was supported by the Centre for Defence Enterprise (CDE) of the UK MoD, project no. CDE 38496. The authors thank Almat Aviation Ltd. for their support in organising and conducting the airborne trials.

7. References

1 Virelli, M., Coletta, A., Battagliere, M.L.: 'ASI COSMO-SkyMed: Mission Overview and Data Exploitation'*IEEE Geoscience and Remote Sensing Magazine*, 2014, **2**, (2), pp. 64–66.

2 Buckreuss, S., Werninghaus, R., Pitz, W.: 'The German satellite mission TerraSAR-X'*IEEE Aerospace and Electronic Systems Magazine*, 2009, **24**, (11), pp. 4–9.

3 Raney, R.: 'RADARSAT-Canada's national radar satellite program'*IEEE Antennas and Propagation Society Newsletter*, 1983, **25**, (3), pp. 4–8.

4 Antoniou, M., Stove, A., Ma, H., *et al.*: 'Passive SAR Satellite Constellation for Near-Persistent Earth Observation: Prospective and Issues'*IEEE Aerospace & Electronic Systems Magazine*, no date, **(in press)**. DOI: 10.1109/MAES.2018.170178

5 Gromek, D., Kulpa, K., Samczyński, P.: 'Experimental Results of Passive SAR Imaging Using DVB-T Illuminators of Opportunity'*IEEE Geoscience and Remote Sensing Letters*, 2016, **13**, (8), pp. 1124–1128.

6 Ulander, L.M.H., Frölind, P.O., Gustavsson, A., Ragnarsson, R., Stenström, G.: 'Airborne passive SAR imaging based on DVB-T signals', in '2017 IEEE International Geoscience and Remote Sensing Symposium (IGARSS)' (2017), pp. 2408–2411

7 Ulander, L.M.H., Frölind, P.O., Gustavsson, A., Ragnarsson, R., Stenström, G.: 'VHF/UHF bistatic and passive SAR ground imaging', in '2015 IEEE Radar Conference (RadarCon)' (2015), pp. 0669–0673

8 Frölind, P.O.: 'Results of airborne passive SAR ground and sea target imaging using DVB-T signals', in '2016 IEEE Radar Conference (RadarConf)' 2016 IEEE Radar Conference (RadarConf), (2016), pp. 1–4

9 Ulander, L.M.H., Frölind, P., Gustavsson, A., Haglund, A., Ragnarsson, R.: 'Passive synthetic-aperture radar for detection of ground vehicles', in 'International Conference on Radar Systems (Radar 2017)' (2017), pp. 1–4

10 Antoniou, M., Cherniakov, M., Hu, C.: 'Space-Surface Bistatic SAR Image Formation Algorithms'*IEEE Transactions on Geoscience and Remote Sensing*, 2009, **47**, (6), pp. 1827–1843.

11 Antoniou, M., Zeng, Z., Feifeng, L., Cherniakov, M.: 'Experimental Demonstration of Passive BSAR Imaging Using Navigation Satellites and a Fixed Receiver'*IEEE Geoscience and Remote Sensing Letters*, 2012, **9**, (3), pp. 477–481.

12 Antoniou, M., Cherniakov, M.: 'GNNS-based passive radar', in Klemm, R. (Ed.): 'Real Aperture Array Radar, Imaging Radar, and Passive and Multistatic Radar' (SciTech Publishing, an imprint of the IET, 2017), pp. 719–766

13 Cherniakov, M. (Ed.): 'Bistatic radar: emerging technology' (Wiley, 2008)

14 Liu, F., Antoniou, M., Zeng, Z., Cherniakov, M.: 'Coherent Change Detection Using Passive GNSS-Based BSAR: Experimental Proof of Concept'*IEEE Transactions on Geoscience and Remote Sensing*, 2013, **51**, (8), pp. 4544–4555.

15 Zhang, Q., Antoniou, M., Chang, W., Cherniakov, M.: 'Spatial Decorrelation in GNSS-Based SAR Coherent Change Detection'*IEEE Transactions on Geoscience and Remote Sensing*, 2015, **53**, (1), pp. 219–228.

16 Santi, F., Bucciarelli, M., Pastina, D., Antoniou, M., Cherniakov, M.: 'Spatial Resolution Improvement in GNSS-Based SAR Using Multistatic Acquisitions and Feature Extraction'*IEEE Transactions on Geoscience and Remote Sensing*, 2016, **54**, (10), pp. 6217–6231.

17 Cazzani, L., Colesanti, C., Leva, D., *et al.*: 'A ground based parasitic SAR experiment', in 'IEEE 1999 International Geoscience and Remote Sensing Symposium. IGARSS'99 (Cat. No.99CH36293)' (1999), pp. 1525–1527 vol.3

18 Kubica, V., Neyt, X., Griffiths, H.: 'Along-track resolution enhancement for bistatic imaging in burst-mode operation'*IEEE Transactions on Aerospace and Electronic Systems*, 2016, **52**, (4), pp. 1568–1575.

19 Ma, H., Stove, A.G., Atkinson, G., Underwood, C.I., Cherniakov, M., Antoniou, M.: 'Passive SAR Using Small Satellite Receivers for Persistent Earth Observation', in IET Radar 2017, (2017)

20 Underwood, C.I., Cherniakov, M., Antoniou, M., Gashinova, M., Stove, A.: 'PASSAT: Passive imaging radar constellation for near-persistent Earth Observation', in 11th IAA conference on small satellites for Earth Observation, (2017)

21 Atkinson, G., Sayin, A., Cherniakov, M., Antoniou, M., Stove, A., Underwood, C.I.: 'Passive SAR Satellite

System (PASSAT): Ground Trials', in International Conference on Radar, (2018)

22 'Spatial FOG | Advanced Navigation', http://www.advancednavigation.com.au/product/spatial-fog, accessed May 2018

23 Searle, S., Palmer, J., Davis, L., O'Hagan, D.W., Ummenhofer, M.: 'Evaluation of the ambiguity function for passive radar with OFDM transmissions', in '2014 IEEE Radar Conference' (2014), pp. 1040–1045

24 Berthillot, C., Santori, A., Rabaste, O., Poullin, D., Lesturgie, M.: 'BEM Reference Signal Estimation for an Airborne Passive Radar Antenna Array'*IEEE Transactions on Aerospace and Electronic Systems*, 2017, **53**, (6), pp. 2833–2845.

25 Soumekh, M.: 'Synthetic aperture radar signal processing with MATLAB algorithms' (J. Wiley, 1999)

26 Antoniou, M., Cherniakov, M.: 'GNSS-based bistatic SAR: a signal processing view'*EURASIP J. Adv. Sig. Proc.*, 2013, **2013**, p. 98.